Kinetic and Thermodynamic Studies of the Folding/Unfolding of a Tryptophan-Containing Mutant of Ribonuclease A[†]

Rebecca A. Sendak, David M. Rothwarf, William J. Wedemeyer, Walid A. Houry, and Harold A. Scheraga*

Baker Laboratory of Chemistry, Cornell University, Ithaca, New York 14853-1301

Received May 31, 1996[⊗]

ABSTRACT: Tryptophan was substituted for Tyr92 to create a sensitive and unique optical probe in order to study the unfolding and refolding kinetics of disulfide-intact bovine pancreatic ribonuclease A by fluorescence-detected stopped-flow techniques. The stability of the Trp mutant was found to be similar to that of wild-type RNase A when denatured by heat or GdnHCl, and the mutant was found to have 85% of the activity of the wild-type protein. Single-jump unfolding experiments showed that the unfolding pathway of the Trp mutant contains a fast and a slow phase similar to those seen previously for the wild-type protein, indicating that the mutation did not alter the unfolding pathway significantly. The activation energy of the slow-unfolding phase suggested that proline isomerization is involved, with the Trp residue presumably reporting on changes in its local environment. Single-jump refolding experiments revealed the presence of a GdnHCl-independent burst phase and a native-like intermediate, most likely I_N, on the folding pathway. Single-jump refolding data at various final GdnHCl concentrations were fit to a kinetic folding model involving two pathways to the native state; one pathway involves the intermediate I_N, and the other is a direct one to the native state. This model provides site-specific information, since Trp92 monitors the formation of local structure only in the neighborhood of that residue. Double-jump refolding experiments permitted the detection of a previously reported, hydrophobically collapsed intermediate, I_Φ. The refolding data support the hypothesis that the region around position 92 is a chain-folding initiation site in the folding pathway.

The unfolded state of disulfide-intact bovine pancreatic ribonuclease A (RNase A)[1] is a mixture of unfolded species (Garel & Baldwin, 1973; Garel et al., 1976; Lin & Brandts, 1983; Schmid, 1983; Houry et al., 1994; Dodge & Scheraga, 1996; Houry & Scheraga, 1996). These unfolded species refold to the native state with different refolding rates, giving rise to multiple refolding phases with different time constants. The unfolded species have been shown to differ in the isomerization state of their X−Pro peptide bonds (Schmid & Baldwin, 1979; Schultz et al., 1992; Houry et al., 1994; Dodge & Scheraga, 1996; Houry & Scheraga, 1996). RNase A contains four proline residues. In the folded state, Pro93 and Pro114 have cis X−Pro peptide bonds while Pro42 and Pro117 have trans X−Pro peptide bonds (Wlodawer et al., 1982, 1988). In the unfolded state, these X−Pro bonds isomerize to form an equilibrium mixture of cis and trans conformations.

Mutants in which each of these prolines was individually replaced by alanine have been studied by Dodge and Scheraga (1996). Folding studies carried out on these mutants indicated that the isomerizations about X−Pro93, -114, and -117 peptide bonds result in the formation of the different unfolded species and affect the refolding kinetics of these unfolded species. Five folding phases have been observed experimentally; these arise from the refolding of the species U_{vf}, U_f, U_m, U_s^I, and U_s^{II}, where U_{vf} and U_f are very-fast- and fast-folding species, respectively. U_m is a medium-folding species, and U_s^I and U_s^{II} are slow-folding species. U_{vf} has all its X−Pro peptide bonds in a native conformation, and represents ∼2−6% of the equilibrium-unfolded state of RNase A (Houry et al., 1994; Dodge & Scheraga, 1996). U_f is postulated to contain a non-native X−Pro114 or -117 peptide bond (Dodge & Scheraga, 1996); it accounts for ∼14% of the unfolded state of the protein (Houry et al., 1994; Dodge & Scheraga, 1996; Houry & Scheraga, 1996). U_{vf} and U_f fold on the millisecond time scale. Recently, Houry et al. (1995, 1996) investigated the refolding pathway of U_{vf}. They found kinetic and thermodynamic evidence for the presence of a hydrophobically collapsed species, I_Φ, on the refolding pathway of U_{vf}.

U_m, U_s^I, and U_s^{II} have refolding time constants which typically occur on the second time scale. All of these species contain non-native X−Pro peptide bond isomers, most significantly at the Tyr92−Pro93 position (Dodge & Scheraga, 1996; Houry & Scheraga, 1996). The folding pathway of the major slow-folding species, U_s^{II}, comprises over 50% of the unfolded state and is thought to form a native-like intermediate, I_N, when folded under favorable folding conditions (Cook et al., 1979; Schmid & Blaschek, 1981; Schmid, 1983, 1986).

The refolding pathway of RNase A has been studied extensively by manual mixing and by stopped-flow fluorescence and absorbance techniques (Tsong et al., 1972; Garel et al., 1976; Lin & Brandts, 1983; Schmid, 1986; Houry et al., 1994). These studies monitor the changes in the optical properties of the intrinsic chromophores that occur during

[†] This work was supported by Grant GM-24893 from the National Institute of General Medical Sciences of the National Institutes of Health. R.A.S. was an NSF predoctoral fellow.

* Author to whom correspondence should be addressed.

[⊗] Abstract published in *Advance ACS Abstracts,* September 15, 1996.

[1] Abbreviations: RNase A, disulfide-intact bovine pancreatic ribonuclease A; GdnHCl, guanidine hydrochloride; NTSB, 2-nitro-5-thiosulfobenzoate; 2′CMP, cytidine 2′-monophosphate.

S0006-2960(96)01280-9 CCC: $12.00

folding or unfolding. A change in the environment of any of the tyrosines upon folding or unfolding directly affects the optical properties of that residue and, therefore, reflects folding or unfolding events occurring at that location of the protein. The experimentally observed changes in absorbance and fluorescence that accompany folding are a sum of the contributions from the individual tyrosine residues. It is difficult to determine the contribution of each specific chromophore to the total absorbance or fluorescence change. In other words, the changes in absorbance or fluorescence that occur during folding do not provide information about specific regions of the protein that are involved in these folding events but instead provide an average view of the change in optical properties of the whole protein.

In order to gain site-specific information about the refolding of RNase A, Tyr92, which precedes Pro93, was replaced by Trp. This site is of interest because Tyr92−Pro93 is involved in a cis peptide bond which reflects itself in the formation of a Type VI β-bend in the native state. This X−Pro peptide group is thought to be important in the folding of RNase A since its isomerization to a trans peptide bond is the origin of the slow folding species of RNase A. Moreover, the presence of the cis peptide bond at that position seems to be essential for the formation of the type VI bend and consequently for the rapid formation of the β-sheet. Even when Pro93 was replaced by alanine, a cis Tyr92−Ala93 peptide bond was formed in the native state of the mutant protein (Dodge & Scheraga, 1996). In addition, Tyr92 is a good candidate for replacement by a probe because it is involved in a hydrogen bond with Asp38 (Scheraga, 1967) in the folded structure. This suggests that the environment of the region containing Tyr92 can be altered during conformational folding (without cis/trans isomerization), leading to a detectable change in the optical properties of this residue. Tyr92 is close to the surface of the protein, which should allow for the accommodation of the slightly larger Trp residue (Wlodawer et al., 1982, 1988).

Since RNase A contains no Trp residues, replacement of Tyr92 by Trp provides a unique probe for that region of the protein. Trp can be excited at wavelengths longer than 295 nm, which do not affect the Tyr residues. In addition, the fluorescence emission of Trp is also distinct from that of Tyr, occurring around 350 nm as opposed to 303 nm. Previous studies involving the observation of single Trp residues within proteins have shown that site-specific information regarding the folding and unfolding pathways can be obtained (Smith et al., 1991; Roper et al., 1992; Bottomly et al., 1994; Steer & Merrill, 1995; Choi et al., 1995; Garcia et al., 1995).

MATERIALS AND METHODS

Materials. Wild-type bovine pancreatic ribonuclease A type 1-A (Sigma) was purified by cation exchange chromatography as described by Rothwarf and Scheraga (1993). The Trp mutant of RNase A was prepared by site-directed mutagenesis using procedures developed previously in our laboratory (Laity et al., 1993). The T7-Gen *in vitro* mutagenesis kit (United States Biochemical) was used to generate the Tyr92 to Trp mutation. The synthetic oligonucleotide used for site-directed mutagenesis was prepared at the Cornell Biotechnology Analytical Facility. The Trp mutant was expressed as a gene 10 fusion protein in the pSJIIGEM-2 vector in HMS174(DE3)-pLys(S). The protein was purified essentially as described by Laity et al. (1993), with the following modification; the initial factor Xa digestion was found to be complete within 6−8 h, rather than 14−18 h. After purification, the Trp mutant RNase A protein was lyophilized and stored over P_2O_5 in a dessicator at 4 °C.

Fluorescence Measurements. Emission spectra of the folded and unfolded Trp mutant were obtained on an MPF-44B Perkin-Elmer spectrophotometer in the ratio mode. In this mode, a portion of the excitation light is diverted before reaching the sample compartment and converted to an electrical signal which is then used to correct the signal from the sample for source lamp intensity fluctuations. The concentration of the Trp mutant was approximately 0.15 mg/mL. Measurements were carried out using a 0.5 × 0.5 cm quartz cuvette. Emission spectra were obtained using excitation wavelengths of 280 and 295 nm with a 2 nm band-pass. Tryptophan and tyrosine are both excited at 280 nm, while only tryptophan is excited at 295 nm. The emission spectra were obtained by scanning the emission wavelength from 280 or 295 to 440 nm at a scan rate of 1 nm/s using a 5 nm band-pass. Each spectrum is the average of three emission scans minus the average of three blank (buffer) scans. The spectra were obtained at the same gain and were scaled by a constant factor which sets the highest fluorescence value at 100, and the fluorescence data are reported using this scale. The maximum fluorescence was found to be at 350 nm (λ_{max}) upon excitation at 280 nm and to occur in the unfolded Trp mutant. This peak fluorescence value was used to scale both of the emission scans (excitation at 280 and 295 nm; Figures 1 and 2).

Activity Measurements. The cleavage of cytidine 2′:3′-cyclic-phosphate (Sigma) was used to measure the enzymatic activity of the Trp mutant and wild-type RNase A at 25 °C and pH 5 and 7 by the method of Crook et al. (1960) as described by Konishi and Scheraga (1980) with modifications described by Laity et al. (1993). Five measurements of the activity of both wild-type and the Trp mutant were made at each pH. The Trp mutant was found to be 84.3 ± 3.5% active at pH 7 and 86.9 ± 3.9% active at pH 5, relative to wild-type RNase A (100%).

Extinction Coefficient Determination. The concentration of wild-type RNase A was determined using an extinction coefficient of 9800 M^{-1} cm^{-1} at 277.5 nm (Sela & Anfinson, 1957). The extinction coefficient of the Trp mutant was determined using an NTSB[1] assay as described previously (Thannhauser et al., 1987). The wavelength of maximum absorbance (λ_{max}) of the Trp mutant was first determined by obtaining an absorbance spectrum of the protein (0.5 mg/mL) in distilled water (pH 4.1). This protein solution was then used in the NTSB assay to determine the extinction coefficient. On the basis of the results of four measurements, the value of the extinction coefficient at 278 nm (λ_{max}) was found to be 14 900 ± 500 M^{-1} cm^{-1} at 25 °C and pH 4.1.

Thermal Transition. The thermal transition was measured for the wild type (0.88 mg/mL) and the Trp mutant (0.56 mg/mL) in 10 mM acetic acid (pH 4.5). The change in absorbance at 287 nm as a function of temperature was measured on a modified Cary model 14 spectrophotometer (Denton et al., 1982). The temperature was raised and lowered in a stepwise manner, allowing 10 min for equilibration at each temperature below 60 °C and 4−5 min for each

temperature above 60 °C. The temperature of the sample cell holder was maintained using a Neslab RTE-100 circulating bath interfaced to a SUN IPC computer. The temperature was measured to within 0.1 °C using a calibrated thermistor placed in a buffer-containing cell located in a second compartment of the cell holder.

Guanidine Hydrochloride Equilibrium Unfolding. The GdnHCl-unfolding transition curves were obtained at 10 °C monitored by fluorescence using a 0.5 × 0.5 cm cell on an MPF-44B Perkin-Elmer spectrophotometer in the ratio mode. The excitation wavelength was 280 nm (3 nm band-pass), and the emission wavelength was 302 nm (5 nm band-pass) to monitor Tyr emission for the wild-type and 350 nm (5 nm band-pass) to monitor mainly Trp emission for the Trp mutant. The measurements were corrected for instrument drift using folded wild-type RNase A in 50 mM acetic acid (pH 5) as a standard. The fluorescence of this standard was found to remain constant during the time required for collection of the GdnHCl transition data. The concentrations of GdnHCl solutions were determined by measuring the refractive index at 25 °C (Nozaki, 1972) using a Bausch & Lomb refractometer. The solutions were filtered through a 0.2 μm filter (Gelman). Solutions were allowed to equilibrate at 10 °C for 2 h prior to measurement. A circulating bath was used to maintain the temperature of the cell at 10.0 ± 0.1 °C. The temperature was measured using a calibrated thermistor (Fisher Scientific). The final fluorescence values were scaled in such a way that the maximum fluorescence in each curve was 100 and the minimum was 0.

Optically Detected Kinetic Experiments. A Hi-Tech Scientific PQ/SF-53 stopped-flow instrument was used to measure fluorescence or absorbance to follow the folding and unfolding kinetics. The instrument has been described previously (Houry et al., 1994). Data were collected every 0.5 ms for the first second and every 40 ms thereafter. Final protein concentrations were approximately 0.15 mg/mL for the Trp mutant and 0.90 mg/mL for wild-type RNase A.

Buffers used for the Trp mutant were sparged with nitrogen to eliminate detectable photo-oxidation of the Trp residue. The excitation wavelength was 295 nm. The emission was monitored at a wavelength range of 320−400 nm using cutoff filters to eliminate any detectable contribution to the fluorescence from tyrosine emission. Solutions of tyrosine and tryptophan with emission spectra identical to those of the folded and unfolded mutant were used to verify the absence of any direct tyrosine fluorescence under these conditions. Essentially no change in absorbance at 295 nm took place during the kinetic experiments.

Unfolding Experiments. Single-jump unfolding experiments were carried out at 10, 15, 20, and 25 °C, respectively, by 6-fold dilution of the folded Trp mutant [0.69 M GdnHCl and 50 mM acetic acid (pH 5.0)] with unfolding buffer [4.9 M GdnHCl and 75 mM glycine (pH 1.8)] to give final conditions of 4.2 M GdnHCl and pH 2.0. Unfolding experiments at pH 5.0 and 10 °C were initiated by 6-fold dilution with unfolding buffer [7.2 M GdnHCl and 50 mM acetic acid (pH 5.0)] to give final conditions of 6.5 M GdnHCl and pH 5.0. The fluorescence of the unfolded species was assigned the value of 100, and that of the folded species was assigned the value of 0. All unfolding data were scaled in this way (see Table 1).

Single-Jump Folding. Single-jump folding experiments were carried out by 11-fold dilution of unfolded protein [4.2 M GdnHCl and 50 mM glycine (pH 2.1)] with folding buffers of varying GdnHCl concentrations [50 mM acetic acid (pH 5.2)] to give solutions of pH 4.9 and final GdnHCl concentrations between 0.58 and 2.6 M. Single-jump folding experiments were repeated under the conditions described above using wild-type RNase A and were monitored by absorbance at 287 nm (Table 2).

Double-Jump Folding. Double-jump experiments (Houry et al., 1994) in which folded RNase A was unfolded for a given amount of time and subsequently refolded were carried out with wild-type RNase A and the Trp mutant at 10 °C. Folded protein [1.5 M GdnHCl and 50 mM acetic acid (pH 5.0)] was diluted 3.5-fold with unfolding buffer [5.3 M GdnHCl and 50 mM glycine (pH 1.7)] to yield unfolding conditions of 4.2 M GdnHCl and pH 2.0. After a given delay time, refolding was initiated by an 11-fold dilution of the unfolded protein with folding buffer [0.2 M GdnHCl and 30 mM acetic acid (pH 5.5)] to yield refolding conditions of 0.58 M GdnHCl and pH 5.0 or by 6-fold dilution [2.3 M GdnHCl and 50 mM acetic acid (pH 5.4)] to yield conditions of 2.5 M GdnHCl and pH 5.0. The delay time was fixed at ∼1 s for the Trp mutant. On the basis of unfolding data at pH 2.0 (Table 1), this delay time is sufficiently long to allow essentially complete conversion of the folded protein to the conformationally unfolded state (U_{vf}) but is short enough so as not to allow for the formation of the other unfolded species.

The value of the fluorescence of conformationally unfolded protein at pH 5.0 and 4.2 M GdnHCl was used as a reference point for later normalization of the refolding data. Because of the possibility of a pH dependence of the fluorescence, the fluorescence emission values used for this normalization were all obtained at pH 5.0. In order to obtain the value for conformationally unfolded protein, the double-jump experiment was repeated; however, the protein was kept unfolded at 4.2 M GdnHCl and pH 5.0 after unfolding at 4.2 M GdnHCl and pH 2 for a set delay time of ∼1 s. The observed fluorescence is that of the conformationally unfolded protein (U_{vf}) at pH 5.

Double-jump folding experiments at 10 °C were repeated with wild-type protein under the same solution conditions used for the Trp mutant. For the wild-type protein, folding was monitored by absorbance (observation at 287 nm) and fluorescence [excitation at 268, observation of emission using cutoff filters (280−400 nm)]. The delay time for experiments with the wild-type protein was set at 0.6 s (Houry et al., 1994) to populate U_{vf} selectively (Table 3).

Inhibitor Binding. The refolding of the Trp mutant was also investigated by monitoring the binding of the inhibitor 2′CMP to the active site during refolding. This experiment was carried out by manual mixing on a Cary 14 spectrophotometer at 10 °C. Unfolded protein [4.2 M GdnHCl and 50 mM glycine (pH 2.0)] was diluted with folding buffer [0.57 M GdnHCl, 50 mM acetic acid (pH 5.3), and 330 μM 2′CMP] to give final folding conditions of 0.92 M GdnHCl, pH 5.0, and 300 μM 2′CMP. Mixing was complete within 10 s. The formation of the 2′CMP complex was monitored by absorbance at 264 nm. The concentration of 2′CMP was determined by using an extinction coefficient of 8770 M^{-1} cm^{-1} at 272 nm, pH 5, and 22 °C (Dodge et al., 1994). The final protein concentration was 36 μM.

Several control experiments were carried out. To conserve recombinant protein, wild-type RNase A was used in many

of these controls at the same protein concentration later used in the experiments with the Trp mutant (36 μM). On the basis of the high level of activity of the Trp mutant, it was assumed that 2′CMP binds to the active site of the Trp mutant in a manner similar to that of the wild-type protein.

First, it was necessary to verify that a sufficient excess of 2′CMP was present to ensure complete binding of RNase A "folded" species. A control experiment, in which the final 2′CMP concentration was 350 μM, exhibited the same total absorbance change at 264 nm as the experiment in which the final 2′CMP concentration was 300 μM. The lack of detection of any additional formation of the complex at the higher 2′CMP concentration indicated that 300 μM 2′CMP was sufficiently high to bind all of the "folded" RNase A present. In a second control experiment, folded wild-type RNase A in 0.92 M GdnHCl was diluted 11-fold with 330 μM 2′CMP in 0.92 M GdnHCl. No change in absorbance at 264 was detected, indicating that the binding of 2′CMP to folded wild-type RNase A is complete within the mixing time. This provided verification that detectable changes in absorbance were due to the formation of folded, or partially folded, protein and not to the binding reaction itself. In a third control experiment, the folding reaction was carried out with buffers that did not contain protein to demonstrate that the absorbance of the 2′CMP alone does not change during the folding reaction.

The change in absorbance of the Trp mutant at 264 nm during folding was observed in the absence of 2′CMP. Small changes in absorbance were detected. To correct for these changes, the average of three 2′CMP binding experiments was fit after the subtraction of the average of three folding runs, monitored at 264 nm, under the same conditions.

Analysis of Kinetic Data. A normalized refolding scale was constructed to analyze and present fluorescence refolding data. The use of this scale was necessary to provide a means of comparing data from the refolding experiments and the double-jump experiments. The fluorescence of the equilibrium-unfolded protein at pH 5 (i.e. protein in 4.2 M GdnHCl at pH 2 that had been diluted with 4.2 M GdnHCl at pH 5.3 to give a solution that was 4.2 M GdnHCl at pH 5) was set to 100, and that of the folded protein at pH 5.0 was set to 0. All of the measurements used to construct this scale were made at pH 5 to eliminate any dependence of the fluorescence on pH. The fluorescence of conformationally unfolded protein (U_{vf}) at pH 5, relative to that of the folded protein (N), was determined in the double-jump experiment through a pH jump under denaturing conditions as described above. The fluorescence of the folded Trp mutant (N) at pH 5 relative to that of the equilibrium-unfolded protein (U) was determined in the single-jump unfolding experiment at pH 5. The fluorescence of the protein was not corrected for GdnHCl dependence, since the GdnHCl dependence of tryptophan fluorescence in model compounds has been observed to be very small at GdnHCl concentrations below 6 M (Edelhoch & Lippoldt, 1969; Kronman & Holmes, 1971). The absence of a GdnHCl dependence of the fluorescence of the Trp mutant in the pre- and post-transition baseline regions (Figure 3) is consistent with this observation. The fluorescence signal of the folded protein solution, however, did increase slightly with increasing GdnHCl concentrations due to scattering from the GdnHCl in solution. To account for the scattering due to GdnHCl, the quantum yield of the folded protein was allowed to vary in the fitting of the data to the model; it was not found to vary significantly.

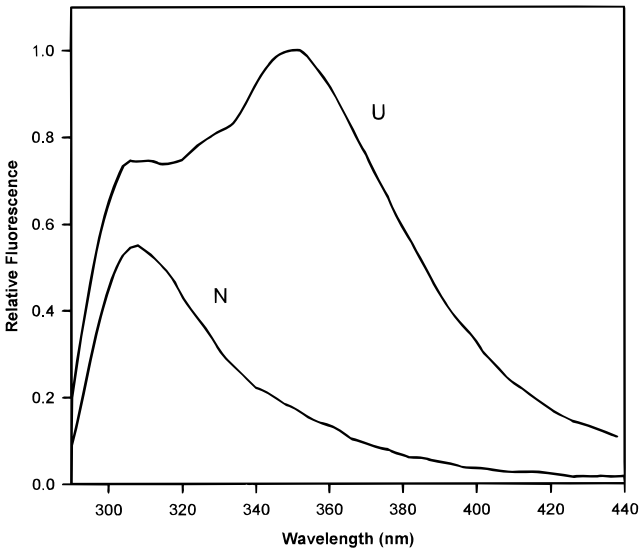

FIGURE 1: Fluorescence emission spectrum of the native (N) and unfolded (U) Trp mutant upon excitation at 280 nm (exciting Trp and Tyr). The spectra were corrected by subtracting blank (buffer) scans and then scaling so that the fluorescence at λ_{max} (350 nm) had a value of 1. The protein concentration was 0.15 mg/mL. Folding buffer: 0.58 M GdnHCl, pH 5. Unfolding buffer: 4.2 M GdnHCl, pH 2.

Double-jump folding data and single-jump unfolding data were fit to exponentials by methods described previously by Dodge et al. (1994). The 95% confidence intervals were determined by the procedure outlined in that paper. The double-jump folding data fit well to a single exponential, and the single-jump unfolding data fit to the sum of two exponentials.

The single-jump folding data obtained for the wild-type and mutant proteins as a function of GdnHCl concentration were fit in this manner (Table 2). For the single-jump refolding data for the Trp mutant, additional analysis was carried out with the ultimate goal of determining the minimum kinetic folding model required to fit the data. For this analysis, two independent methods were used to find the minimum number of exponentials that could fit the single-jump folding decay curves (see Appendix). This analysis indicated that two exponentials and a constant were sufficient to model the single-jump fluorescence data, except at the highest GdnHCl concentration (2.6 M), where one exponential and a constant were sufficient. The data at 0.58 M GdnHCl were not included in the fit to the model because the mixing artifacts were larger than those seen at other GdnHCl concentrations. The χ^2 values were typically well within the assigned tolerance. A model based on this analysis is presented in the Discussion section.

RESULTS

Fluorescence of the Trp Mutant. The emission of both tryptophan and tyrosine is evident in the fluorescence emission spectra of the unfolded Trp mutant upon excitation at 280 nm (Figure 1). Two maxima are seen corresponding to the fluorescence of tyrosine, which is centered around 302 nm, and to that of tryptophan, which is centered around 350 nm. The emission of tyrosine is evident in the native spectrum (not shown here); however, that of tryptophan is

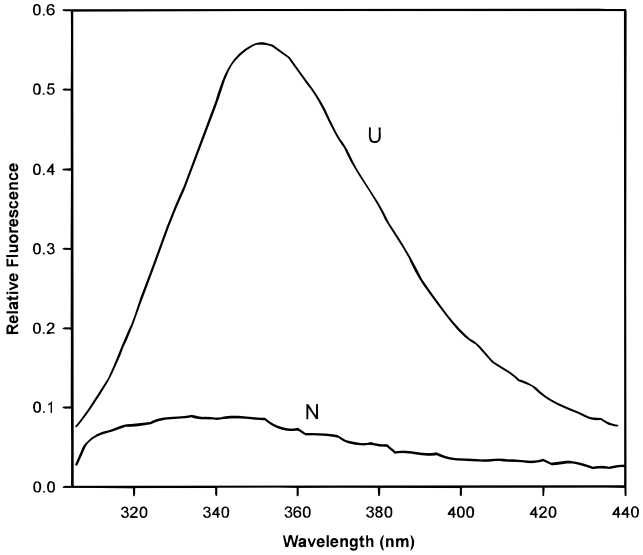

FIGURE 2: Fluorescence emission spectrum of the native (N) and unfolded (U) Trp mutant upon excitation at 295 nm (exciting only Trp). Fluorescence was corrected and scaled relative to the maximum when excited at 280 nm. The protein concentration was 0.15 mg/mL. Folding buffer: 0.58 M GdnHCl, pH 5. Unfolding buffer: 4.2 M GdnHCl, pH 2.

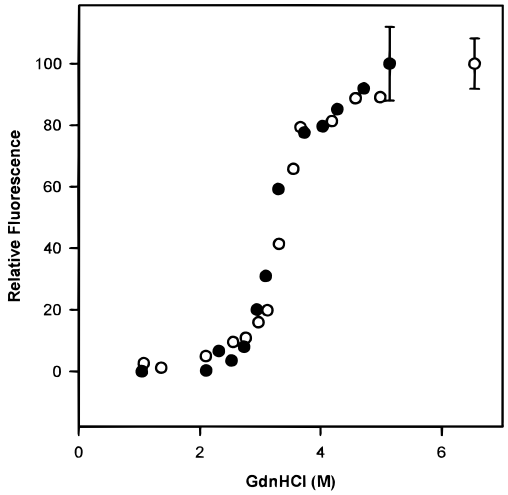

FIGURE 3: Fluorescence-detected GdnHCl equilibrium unfolding transition of Trp mutant (○) and wild-type (●) RNase A measured by the change in fluorescence (Trp mutant, emission at 350 nm; and wild-type, emission at 302 nm) upon excitation at 280 nm at pH 5 and 10 °C. Each curve was scaled in such a way that the maximum fluorescence is 100 and the minimum is 0. Error symbols represent the average standard deviation of three measurements taken at each concentration of GdnHCl.

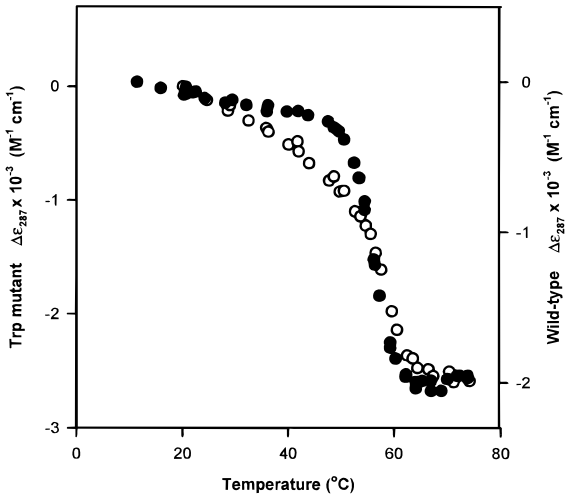

FIGURE 4: Absorbance-detected thermal transition of Trp mutant (○) and wild-type (●) RNase A at pH 4.5 measured by the change in absorbance at 287 nm. The concentration of the Trp mutant was 0.56 mg/mL, and that of the wild type was 0.88 mg/mL.

not apparent. When the Trp mutant is excited at 295 nm, only Trp emission is observed and little emission from the Tyr residues is detected (Figure 2). This is because Tyr does not absorb significantly at 295 nm. Therefore, the selective excitation of Trp92 is possible at 295 nm.

The fluorescence of the unfolded Trp mutant at 350 nm (λ_{max}) is approximately 10-fold larger than that of the folded protein at 350 nm (Figures 1 and 2). The quenching of the Trp fluorescence indicates that it participates in some interaction with other residue(s), in the folded native structure. This cannot be attributed solely to burial since the fluorescence spectrum of Trp reflects interactions with the surrounding residues, and changes can arise as a result of subtle differences in the microenvironment. There appears to be no significant correlation between the quantum yield of Trp and its solvent accessibility (Eftink, 1991). However, in general, shifts in λ_{max} of a Trp residue between the folded and unfolded protein do provide an indication of the relative polarity of the environment of the residue in the folded and unfolded states (Leach & Scheraga, 1960; Burstein et al., 1973). The low fluorescence in the folded Trp mutant (Figure 2), however, prevents the identification of a clear λ_{max} for the folded protein.

Stability of the Trp Mutant. The Trp mutant and wild-type protein showed similar GdnHCl and thermal transition curves (Figures 3 and 4, respectively). The thermal transition of the Trp mutant (Figure 4) exhibits a significant slope in the pre-transition region. The absorbance of the Trp mutant is dominated by the Trp residue. The significant slope in the pre-transition region is probably due to the high sensitivity of Trp92 to its environment. In addition to reflecting global unfolding, the absorbance of the Trp residue may also be reporting a local event such as a slight expansion in that portion of the protein in the pre-transition region.

The values of $(GdnHCl)_{1/2}$ (midpoint of the GdnHCl transition) and T_m (midpoint of the thermal transition) were calculated using the procedure described by Pace et al. (1989). The errors in these values were estimated using the errors in the slopes and intercepts of the pre- and post-transition regions. The values of $(GdnHCl)_{1/2}$ for the wild-type and the Trp mutant were determined to be 3.2 ± 0.3 and 3.4 ± 0.2 M, respectively. The T_m for the wild type was 56.3 ± 3.1 °C, and that of the Trp mutant was 58.0 ± 2.8 °C. The similarities in these values suggest that the substitution of Trp for Tyr does not alter the stability of RNase A.

Unfolding Experiments. Two phases were observed when the protein was unfolded at 4.2 M GdnHCl and pH 2.0 between 5 and 25 °C (Table 1, Figure 5). These phases are referred to as the fast- and slow-unfolding phases. The fast phase (Figure 5A), which reflects conformational unfolding from N to U_{vf}, represents 25−30% of the total fluorescence change and has an activation energy of 19.2 kcal/mol. The slower phase (Figure 5B) has an activation energy of 21.4 kcal/mol. The fast phase folds on the millisecond time scale, while the slower phase folds on the seconds to minutes time

Table 1: Time Constants and Relative Amplitudes for the Unfolding of the Trp Mutant at Various Temperatures[a]

final pH	final [GdnHCl] (M)	temperature (°C)	τ_f (s)	τ_s (s)	amplitude[b] of τ_f	amplitude[b] of τ_s
2.0	4.2	5	0.165 ± 0.001[c]	897 ± 13	29.6 ± 0.1	70.4 ± 0.5
2.0	4.2	10	0.0953 ± 0.007	450 ± 4	29.5 ± 0.1	70.5 ± 0.2
2.0	4.2	15	0.0546 ± 0.007	234 ± 2	28.9 ± 0.2	71.1 ± 0.2
2.0	4.2	20	0.0291 ± 0.006	123 ± 1	28.2 ± 0.3	71.8 ± 0.2
2.0	4.2	25	0.0162 ± 0.006	66.4 ± 0.6	25.7 ± 0.6	74.3 ± 0.4
5.0	6.5	10	20.2 ± 1.4	326 ± 7	20.4 ± 0.7	79.6 ± 0.5

[a] Obtained by stopped-flow fluorescence measurements: excitation at 295 nm and observation of emission at 320−400 nm. [b] The sum of the amplitudes was set at 100 for each data set at a particular pH and temperature. [c] The error is calculated at the 95% confidence limit.

Table 2: Time Constants and Amplitudes for Single-Jump Refolding at 10 °C and pH 5.0.

	wild-type RNase A[a]				Trp Mutant RNase A[b]			
final [GdnHCl] (M)	τ_1 (s)	amplitude of τ_1[c]	τ_2 (s)	amplitude of τ_2[c]	τ_1 (s)	amplitude of τ_1[c]	τ_2 (s)	amplitude of τ_2[d]
0.58	29.5 (28.7−30.5)	76.8 (75.3−78.9)	148 (137−168)	23.2 (21.3−24.8)	22.5 (21.9−23.2)	53.7 (52.3−55.1)	89.1 (88.2−89.9)	103.9 (102.5−105.4)
0.90	52.6 (45.6−59.2)	58.4 (48.3−68.5)	156 (137−186)	41.6 (31.2−52.0)	40.0 (38.3−41.7)	38.7 (37.4−40.2)	135 (133−137)	87.9 (86.5−89.5)
1.22	101 (88.5−118)	38.9 (30.5−49.2)	282 (257−309)	61.1 (50.9−69.6)	55.4 (53.9−56.9)	21.1 (20.7−21.7)	260 (258−261)	72.4 (71.9−72.9)
1.78			522 (504−538)		80.4 (74.0−87.6)	8.3 (8.0−8.8)	603 (596−609)	59.8 (59.5−60.2)
2.16			699 (654−719)		125 (110−143)	5.0 (4.6−5.4)	834 (824−844)	57.4 (57.0−57.9)
2.61			1120 (1100−1140)				1250 (1240−1270)	53.7 (53.1−54.0)

[a] Obtained by stopped-flow absorbance measurements at 287 nm; amplitudes are expressed as a percent of the total refolding value. The error range, shown in parentheses, is calculated at the 95% confidence limit. [b] Obtained by stopped-flow fluorescence measurements: excitation at 295 nm and observation of emission at 320−400 nm; amplitudes are expressed in normalized units as described in the text. The burst phase accounts for approximately 50% of the refolding value. [c] Amplitude is positive, i.e. fluorescence (or absorbance) increases with time. [d] Amplitude is negative, i.e. fluorescence decreases with time.

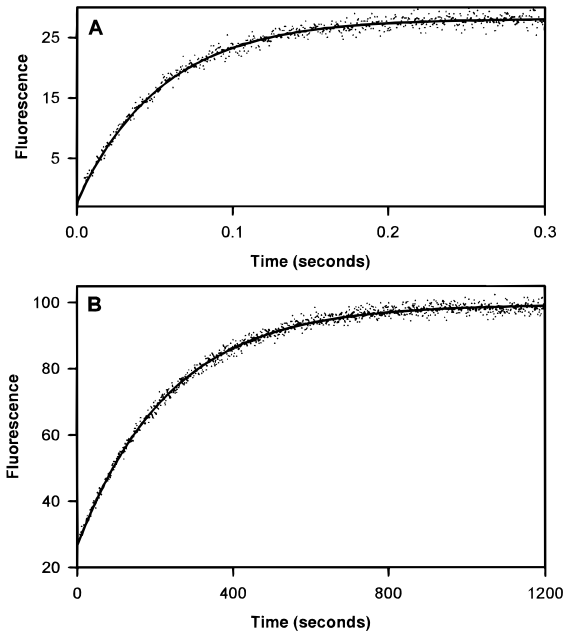

FIGURE 5: Representative data set showing the change in fluorescence at 350 nm upon unfolding of the Trp mutant from 0.7 M GdnHCl (pH 5.0) to 4.2 M GdnHCl (pH 2.0) at 15 °C. The fast phase (A) and slow phase (B) are shown. Excitation was at 295 nm, and the emission was observed between 320 and 400 nm.

scale (Table 1). This is consistent with observations by Houry et al. (1994) for wild-type RNase A under similar conditions. The activation energy of proline isomerization is ~20 kcal/mol, and the time constant varies from tens to thousands of seconds depending on the experimental conditions (Nall, 1985). The time constant and activation energy of the slow phase indicate that proline isomerization is taking place. Although the activation energy of the fast phase is similar, it occurs on a time scale that is too fast for it to be proline isomerization.

Two unfolding phases were also observed when the protein was unfolded at 6.5 M GdnHCl and pH 5.0 at 10 °C (Table 1). Under these conditions, the time constant of the fast phase is ~20 s instead of ~100 ms as is the case for unfolding at 4.2 M GdnHCl and pH 2.

Single-Jump Folding Experiments. As shown in Table 2, two phases were observed under all conditions used to monitor the folding of the Trp mutant except at 2.6 M GdnHCl. No fast-folding phase was detectable at 2.6 M GdnHCl within the first second of folding. The refolding reaction at all final GdnHCl concentrations except 2.6 M was characterized by a large initial quenching of fluorescence (relative to the unfolded protein at 4.2 M GdnHCl and pH 5) during the dead time of mixing which is estimated to be ~2 ms (Houry et al., 1994), followed by an increase in fluorescence (first phase) and finally a decay with decreasing fluorescence to the folded state (second phase) (Figure 6). The amplitude of the faster phase decreases with increasing GdnHCl concentrations; at 2.6 M GdnHCl the fast phase is absent altogether (Table 2). The magnitude of the (negative) amplitude of the slower phase also decreases with increasing GdnHCl concentrations such that the sum of the amplitudes of the two exponential processes (i.e. the burst phase) is

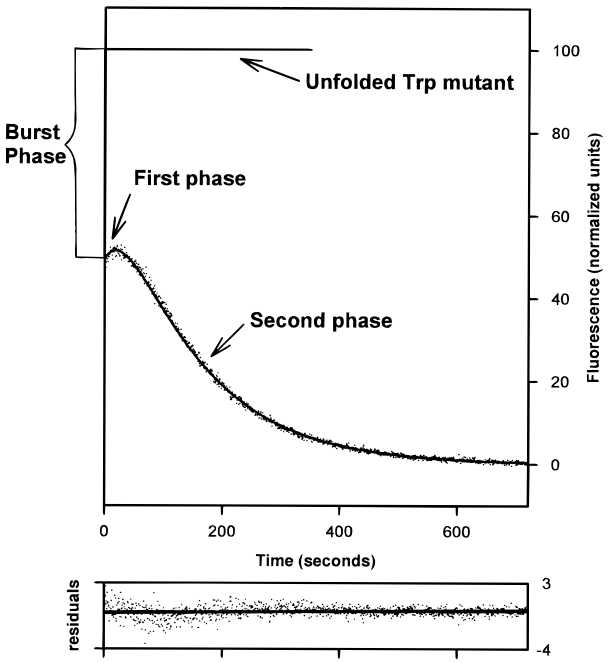

FIGURE 6: Representative data set showing the change in fluorescence at 350 nm upon refolding of the Trp mutant from the equilibrium-unfolded state at 10 °C. Excitation was at 295 nm, and emission was observed between 320 and 400 nm. Protein at 4.2 M GdnHCl (pH 2.0) was refolded at final conditions of 0.90 M GdnHCl and pH 5.0. The data are shown on a normalized scale. The fluorescence of the unfolded Trp mutant at 4.2 M GdnHCl (pH 5) was set at a fluorescence value of 100 (line), and the fluorescence of the folded Trp mutant was set at a value of 0. The fast (first) phase is the folding phase with increasing fluorescence, and the slow (second) phase is that with decreasing fluorescence. The burst phase is the difference between the fluorescence of the unfolded protein at 4.2 M GdnHCl and pH 5.0 and the initial fluorescence after the dead time of mixing.

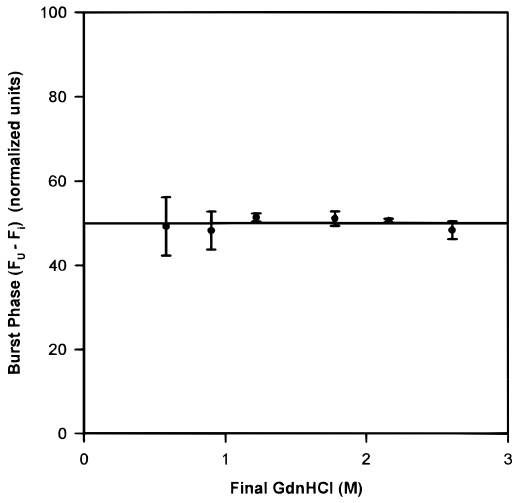

FIGURE 7: Magnitude of the burst phase upon refolding of the equilibrium-unfolded Trp mutant at 10 °C. The burst phase is the difference between the fluoresence of the unfolded protein at 4.2 M GdnHCl and pH 5.0 (F_u) and the fluorescence measured immediately after the dead time of mixing (F_i) also at pH 5.0 and the GdnHCl concentration indicated on the abscissa. Each point is the average of three or more individual measurements, and the standard deviation is reflected by the error symbols.

constant. From Table 2, it can also be seen that the absorbance-detected refolding of the wild-type protein exhibits qualitatively similar properties.

The initial quenching of fluorescence of the Trp mutant, which occurs in the dead time of the instrument, is referred to as the burst phase. The magnitude of the initial burst phase during which quenching took place was independent of the final GdnHCl concentration (Figure 7). The magnitude of the burst phase is approximately 50 under all of the experimental conditions, signifying that half of the unfolded fluorescence becomes quenched in the dead time of mixing (see Materials and Methods for discussion of the normalized scale).

Two folding phases were observed when refolding was monitored by 2′CMP binding under final conditions of 0.90 M GdnHCl and pH 5. Whereas τ_1 is 40 s when the process is monitored by the change in fluorescence (Table 2), it was ~10 s when monitored by 2′CMP binding. An apparent increase in the rate constant for the folding of the major slow phase of wild-type RNase A when measured by 2′CMP binding, as compared to the rate constant measured by the change in tyrosine absorbance, has been reported previously by Dodge et al. (1994). The acceleration in rate that we observe is somewhat larger than that seen by Dodge et al. (1994). This could be due to the fact that our studies are carried out at a higher GdnHCl concentration, that we are studying a mutant protein, or that the 2′CMP binding constant has not been used to correct for the depletion of 2′CMP during the folding reaction. The ~10 s phase accounted for approximately 70% of the amplitude, while the remaining 30% was found to have a time constant of ~136 s. These phases appear to correspond to the first and second phases seen by fluorescence-detected refolding (Table 2).

Double-Jump Experiments. A fast-refolding phase was detected after unfolding the Trp mutant for ~1 s and subsequently refolding at 2.50 M GdnHCl and pH 5.0 and 0.58 M GdnHCl and pH 5.0 (Table 3). This phase was faster

Table 3: Time Constants and Amplitudes for Double-Jump Refolding at 10 °C and pH 5.0

	wild-type RNase A		Trp mutant RNase A		
			fluorescence[c]		
final [GdnHCl] (M)	absorbance[a] τ (ms)	fluorescence[b] τ (ms)	τ (ms)	amplitude[d] of the observed phase	amplitude[d] of the burst phase
0.58	27.2 (25.8−28.8)[e]	22.8 (21.5−23.9)	18.3 (16.6−20.3)	5.66 (5.20−6.15)	14.6
2.50	1730 (1711−1757)	1831 (1745−1922)	894 (849−942)	12.6 (12.2−13.0)	8.29

[a] Obtained by stopped-flow absorbance measurements at 287 nm. [b] Obtained by stopped-flow fluorescence measurements: excitation at 268 nm and observation of emission at 280−400 nm. [c] Obtained by stopped-flow fluorescence measurements: excitation at 295 nm and observation of emission at 320−400 nm. [d] Amplitudes are expressed in normalized units as described in the text. [e] Error range calculated at the 95% confidence limit.

than that of the wild type when monitored by either fluorescence or absorbance. A burst phase (quenching during the dead time of mixing) was observed. The burst phase seen in the double-jump experiments has some guanidine dependence (see Table 3).

DISCUSSION

Unfolding Studies. The experimentally observed unfolding phases (Table 1) of the Trp mutant are similar to those detected for wild-type unfolding under comparable conditions (Houry et al., 1994; Rehage & Schmid, 1982). A fast phase which corresponds to conformational unfolding and a slow phase which corresponds to proline isomerization are seen, as with the wild type. This suggests that the mutation of Tyr to Trp has not significantly altered the unfolding pathway of RNase A and that the Trp residue is reporting on changes in its local environment (i.e. the isomerization of the Trp92−Pro93 peptide bond). It is, however, interesting to note that the time constant for the slow phase is significantly shorter at pH 5 and 10 °C than at pH 2 and 10 °C (column 5 of Table 1). This could be due to the different pH at which the measurements were made or to the different GdnHCl concentrations used. The rate of proline isomerization in an unfolded protein is generally thought to be insensitive to both denaturant concentration and pH (Nall, 1985). The most likely explanation is that there are some specific local interactions between Trp92 and Pro93 which are affected by the difference in the GdnHCl concentration. This then leads to the differences in the apparent relaxation times for the cis/trans isomerization process. Supporting this view is the observation that the values of the time constant for the slow-unfolding phase (τ_s) of the Trp mutant at pH 2.0 are ∼3-fold larger than the time constants reported by Houry et al. (1994) for wild-type RNase A under the same solution conditions. Further evidence for the presence of specific Trp−Pro interactions is presented in the following section.

It is also interesting to note that the time constant for the fast phase conformational unfolding (τ_f) of the Trp mutant at pH 2.0 is significantly larger (∼1.5−2-fold) than that reported by Houry et al. (1994) for the wild-type protein under the same conditions. This indicates that the native state of the Trp mutant is more stable relative to its transition state than is wild-type RNase A. It would appear unlikely that the Trp mutation would increase the free energy of the transition state through interactions not found in the native state. Therefore, we must conclude that the presence of Trp92 lowers the free energy of the native state relative to its transition state through interactions present in the native state.

Burst Phase: Single-Jump Refolding. The presence of a burst phase, or a difference between the initial fluorescence and that of the unfolded mutant protein, is evident in the single-jump refolding data (Figure 6, Table 3). This indicates that some folding event corresponding to the formation of structure, which is not present under unfolding conditions, occurs in the dead time of mixing. In the absence of such effects, the initial fluorescence measured immediately upon folding would correspond to the fluorescence of the unfolded state at pH 5. The burst phase was found to be independent of the final GdnHCl concentration (Figure 7). This suggests two possible explanations. One is that the intermediate formed during the burst phase is so stable that, even at 2.6 M GdnHCl, it is not appreciably denatured. The second possibility is that the intermediate is stabilized by local interactions that are very insensitive to GdnHCl. Kemmink and Creighton (1995) have recently described an interaction between Tyr and Pro which is essentially GdnHCl-independent. In their studies of short peptides, they identify by NMR spectroscopy several enthalpic interactions of the side chains of Phe or Tyr with Pro and Gly. These interactions were affected only slightly by GdnHCl and urea. It is possible that interactions of this type occur between Trp92 and Pro93 and account for the burst phase, as noted in the previous section.

Burst Phase: Double-Jump Refolding. A burst phase is also present in the double-jump experiments under both final refolding conditions. The burst phase is larger at 0.58 M GdnHCl but is still present at 2.5 M GdnHCl (Table 3). This dependence of the double-jump burst phase on GdnHCl suggests that it may be the hydrophobically collapsed intermediate, I_Φ, that is being detected (Houry et al., 1995). The evidence for the existence of this intermediate came from kinetic and thermodynamic calculations based on the behavior of the very fast phase under a variety of conditions. I_Φ has recently been observed directly in stopped-flow CD studies (Houry et al., 1996).

The ability to detect I_Φ in the folding of the Trp mutant suggests that this region of RNase A is buried in this hydrophobically collapsed intermediate. In a recent study of Pro mutants, Dodge and Scheraga (1996) provided experimental evidence for the hypothesis of Matheson and Scheraga (1978) and Montelione and Scheraga (1989) that this region of wild-type RNase A is part of a chain-folding initiation site.

The two folding conditions that were chosen for the double-jump experiment are of interest for the following reason. Houry et al. (1995) found evidence for the existence of I_Φ at 0.58 M GdnHCl, but not at 2.5 M GdnHCl. If the burst phase seen in the double-jump experiments of the Trp mutant arises solely from the formation of I_Φ, it would be undetectable at 2.5 M GdnHCl. However, the presence of a burst phase at 2.5 M GdnHCl is observed (Table 3). It is possible that I_Φ is, in fact, observed for the mutant at 2.5 M GdnHCl; the presence of Trp92 may in some way stabilize the I_Φ intermediate against denaturation by GdnHCl. Alternatively, the burst phase seen at 2.5 M GdnHCl may indicate the presence of a different intermediate that is less sensitive to GdnHCl. One possibility is that I_U, an intermediate that has been described recently by Houry et al. (1996), is the one detected. This intermediate, which forms prior to I_Φ, was detected by stopped-flow CD experiments; it is largely unfolded but contains some local structure.

Fast-Folding Species. In the folding pathway of wild-type RNase A, two fast-folding species, U_f and U_{vf}, account for ∼24% of the change in the absorbance amplitude and ∼13% of the change in the fluorescence amplitude (Houry et al., 1994). The single-jump refolding experiments of the Trp mutant do not show the presence of any fast-folding phases. This does not necessarily mean that these phases are absent, however. The ability to observe the fast phases depends upon whether the fluorescence change upon folding of these phases is above the experimental detection limit. In order to determine what percentage of the unfolded population could be in the U_{vf} and U_f states without detection of a

change in fluorescence upon folding, the double-jump data and single-jump refolding data were analyzed. Since the two states differ only in the isomerization state of either Pro114 or Pro117 (Dodge & Scheraga, 1996), both of which are remote from Trp92, then the quantum yields of U_{vf} and U_f at 350 nm (due to Trp) should be the same. Thus, any information obtained regarding the magnitude of the fluorescence change upon folding of either species should be applicable to the other.

The double-jump data were used to determine the magnitude of the change in fluorescence upon folding of the fast phases under conditions in which they are populated. The first step in the double-jump experiment involved unfolding for a given delay time. The unfolding data were used to select a delay time that would allow essentially complete population of the conformationally unfolded state (U_{vf}). Subsequently, the refolding of approximately 100% of the population in the U_{vf} state was observed. This provided a direct measure of the magnitude of the change in fluorescence for a given population undergoing the U_{vf}-to-native folding event; the folding of approximately 100% of U_{vf} accounted for at most 13% of the normalized folding fluorescence scale (see Materials and Methods for a discussion of the normalized scale).

The refolding data were then examined to determine the detection limit. The refolding data obtained at 2.6 M GdnHCl were chosen for the analysis, as opposed to those at 0.58, because the fast phase would be slower and thus more easily detected and also would have the largest amplitude (Table 3). The detection limit was taken to be 3 times the standard deviation in the data (Kaiser, 1970). This limit was found to be approximately 2.6% of the normalized scale. On the basis of the information obtained from the double-jump experiments, each 1% of U_{vf} (or U_f) accounts for a 0.13% fluorescence change on the normalized scale. With a detection limit of 2.6% in the single-jump refolding experiment, as much as 20% of the population could be present as U_f and U_{vf}. Therefore, because of the small relative fluorescence change upon the folding of the fast-folding species, up to 20% of the population of the equilibrium-unfolded Trp mutant refolding through the U_f pathway would be undetectable within the noise in the data.

Single-Jump Folding Model. It is of interest to model the single-jump refolding data for the Trp mutant using a minimal model. As described in Materials and Methods, the minimum number of exponentials to which those data can be fit is two (see Appendix). Consequently, the minimal model which can fit the single-jump fluorescence refolding data must contain three species (U′, I_N, and N) with interconversion rate constants on an experimentally measurable time scale. The most general model that is consistent with our data is shown in Figure 8.

In this model, U collapses during the burst phase into U′, a process described by an immeasurable rate constant k_{burst}. U′ folds either directly to the native protein (N) or through an intermediate I_N. Given that all of the experiments are carried out under folding conditions where N is not expected to unfold significantly (see Figure 3), no unfolding processes from N have been included.

Several assumptions are involved in the designation of the species in this model. First, the intermediate that is formed in the burst phase has been labeled U′ since, as discussed

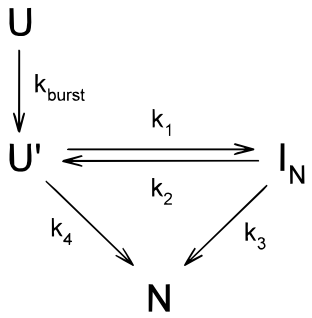

FIGURE 8: Assumed model for the folding/unfolding kinetic data. The first and second rate constants (k_1 and k_2, respectively) were assumed to have a linear dependence on the GdnHCl concentration, and the third and fourth rate constants (k_3 and k_4) were allowed to vary in the fitting of the data.

previously, the state from which refolding is started *after* the dead time of mixing is not the same as the equilibrium-unfolded state at 4.2 M GdnHCl and pH 2 (labeled U). The rate at which U collapses to U′ (k_{burst}) is immeasurably fast and thus was not included in the fitting of the data to the model. Second, we have referred to the intermediate as I_N and not simply as I. This is based on the inhibitor binding data which indicate that the species formed in the fast decay process is native-like. The amplitude of the first (fast) decay process decreases as the GdnHCl concentration increases and disappears at 2.6 M GdnHCl (see Table 2). As discussed in the introductory section, a native-like intermediate that can bind the inhibitor with the same affinity as that of the wild-type protein has previously been observed to form in the major slow-refolding pathway (Cook et al., 1979; Schmid, 1981; Schmid & Blaschek, 1981). This intermediate has been shown to become destabilized at increasing GdnHCl concentrations and is essentially not present above 2 M GdnHCl and pH 6 (Schmid, 1983). This intermediate has been labeled I_N.

The kinetic model can be treated analytically. The experimentally observed fluorescence intensity as a function of refolding time, $F(t)$, is expressed in eq 1.

$$F(t) = A_1 e^{-\lambda_1 t} + A_2 e^{-\lambda_2 t} + F_\infty \qquad (1)$$

where A_1 and A_2 are the amplitudes of the first and second phases, respectively, λ_1 and λ_2 are the first (fast) and second (slow) decay rate constants, respectively, and F_∞ is a constant. The observed amplitudes and decay rate constants are related to the quantum yields and reaction rates of the model by five simple equations (eqs A-4−A-8 of the Appendix).

The data obtained at a single GdnHCl concentration do not contain sufficient information to fit the parameters uniquely in eqs A-4−A-8; proper fitting of the data requires the use of *all* of the single-jump fluorescence folding data obtained at five different GdnHCl concentrations. In order to use these data, we must select the proper functional form with which to express the GdnHCl dependence of the various parameters. As discussed previously, the assumption that the quantum yield of Trp is insensitive to GdnHCl is reasonable; hence, Q_N, Q_{I_N}, and Q_U in eqs A-4, A-5, and A-8 will be considered to be independent of GdnHCl concentration.

The proper choice of the functional form for the GdnHCl dependence of the rate constants depends on further interpretation of our model. Since the formation of I_N involves

formation of native-like structure, the equilibrium constant between U′ and I_N, k_1/k_2, can be treated in a manner analogous to that of the equilibrium folding/unfolding of proteins. There are many models to describe the GdnHCl dependence of the refolding/unfolding equilibrium process (Pace, 1986; Schellman, 1987; Alonso & Dill, 1991). The most commonly used model is the linear one in which the log of the equilibrium constant depends linearly on the concentration of GdnHCl. By the use of transition state theory, this equilibrium model can be extended to rate constants:

$$\ln k_i = \ln k_i^0 - m_i^{\ddagger}\frac{[\text{GdnHCl}]}{RT} \qquad (2)$$

where R is the gas constant, T is the absolute temperature, k^0 represents the value of the rate constant in the absence of GdnHCl, and $m^{\ddagger}$ is a constant proportional to the solvent-exposed surface area that becomes buried or exposed in the transition. We, therefore, can use this expression for the GdnHCl dependence of k_1 and k_2. In this case, since k_1 corresponds to a folding step, $m_1^{\ddagger}$ will be a positive number, and since k_2 corresponds to an unfolding step, $m_2^{\ddagger}$ will be a negative number. We assume that the transition state between U′ and I_N, the same as that between I_N and U′, does not change with GdnHCl concentration; therefore, $m_1^{\ddagger}$ and $m_2^{\ddagger}$ will be GdnHCl-independent quantities. For k_3 and k_4, we have no knowledge of the process(es) involved other than that it must in some way involve isomerization of X−Pro peptide bonds. We, therefore, will apply no GdnHCl-dependent constraints to these two rate constants and treat them as variables in the fitting of the model to the data.

The model, subject to the constraints described above, was fit to all of the single-jump refolding fluorescence data as described in the Appendix. The final reduced χ^2 for the fitting was 0.99; hence, the data are fit well by the proposed model. The rate constants obtained from the fit are shown in Figure 9 as a function of GdnHCl concentration along with their errors at 95% confidence. While a linear dependence of ln k_1 and ln k_2 on the GdnHCl concentration is required by the model (the slope and intercept are variables), ln k_3 and ln k_4 are also found to exhibit a linear dependence on the GdnHCl concentration.

Comparison of the Folding of the Trp Mutant to That of Wild-Type RNase A. The model has only one unfolded species, U′, that gives rise to the change in fluorescence upon folding (after the burst phase). This is in contrast to the refolding of wild-type RNase A for which five refolding phases have been shown to arise from eight different unfolded species with X−Pro peptide bonds that differ in their state of isomerization (Dodge & Scheraga, 1996; Houry & Scheraga, 1996). U_{vf} and U_f cannot be detected in our fluorescence-detected folding studies of the Trp mutant because the change in fluorescence upon folding of these species is very small; therefore, they can be ignored in the comparison. This still leaves three slow phases that are observed in the refolding of wild-type RNase A to be accounted for. On the basis of double-jump and proline mutation studies, the three slow-folding species, U_s^I, U_s^{II}, and U_m, with a trans Tyr92−Pro93 peptide bond have relative populations of 17, 76, and 7%, respectively (Houry & Scheraga, 1996) (the Trp mutation should in no way affect these values since they pertain to the relative population of cis/trans X−Pro peptide bonds preceding Pro114 and Pro117 which should be unaffected by Trp92 in the unfolded state).

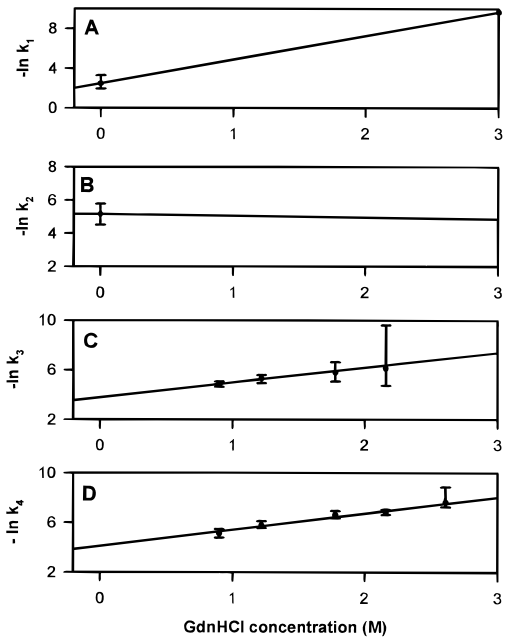

FIGURE 9: GdnHCl dependence of the rate constants of the minimal model discussed in the text. (A) The dependence of $-\ln k_1$ is shown with the error in the intercept; the slope ($m_1^{\ddagger}$) was found to be 1.22 kcal mol^{-1} M^{-1} (95% confidence range; 1.07−1.45 kcal mol^{-1} M^{-1}). (B) The dependence of $-\ln k_2$ is shown with the error in the intercept; the slope ($m_2^{\ddagger}$) was found to be −0.097 kcal mol^{-1} M^{-1} (95% confidence range; −0.334 to 0.219 kcal mol^{-1} M^{-1}). (C) The dependence of $-\ln k_3$, and (D) the dependence of $-\ln k_4$, on GdnHCl concentration are shown together with the calculated error symbols (95% confidence).

The results in Table 2 show that the folding data for wild-type and Trp mutant RNase A are qualitatively similar. An exact comparison cannot be made, however, because the model to which the Trp mutant data were fit is very simple compared to that which describes the folding of wild-type RNase A; previous studies in our laboratory (Houry et al., 1994; Dodge et al., 1996) demonstrate that the absorbance-detected folding of wild-type RNase A is more complex than can be fitted with this minimal model. This is because the process being monitored by absorbance or fluorescence in the folding of wild-type RNase A is the formation of native protein. In contrast, Trp92 in the Trp mutant monitors only the formation of local structure in the neighborhood of that residue.

The minimal model discussed above does not explicitly distinguish the U_s^I and U_s^{II} species observed in wild-type ribonuclease A folding. Two kinetic models incorporating these species were investigated (panels A and B of Figure 10). These models were difficult to fit since they predict three decaying exponentials in the fluorescence data (even if the quantum yields of U_s^I and U_s^{II} are identical), while only two exponentials were discernible in our data, using two independent tests (see the Appendix). Numerical fitting to these models showed that these models are underdetermined by our data, e.g. yielding hundred-fold larger errors in the rate constants. However, both models are consistent with the data and cannot be ruled out. Future experiments will determine the range of conditions under which the minimal model describes the refolding of the Trp mutant

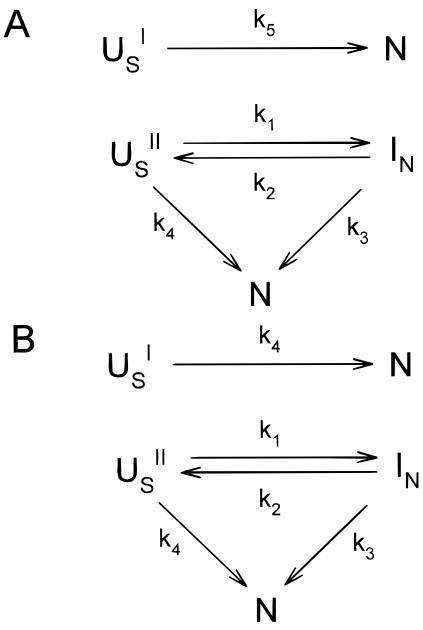

FIGURE 10: (A and B) Two complex kinetic models for the folding/refolding of the Trp mutant; they differ only in the magnitude of the rate constant for the $U_s^I \rightarrow N$ step. These models were found to be consistent with the Trp mutant fluorescence data, but their parameters were underdetermined.

and clarify its relationship to more detailed models, e.g. the 16-species box model (Houry & Scheraga, 1996).

Nature of I_N. Interestingly, the equilibrium *m* value [*m* (from eq 2) $= m_1^{\ddagger} - m_2^{\ddagger}$] for the $U' \rightleftharpoons I_N$ process of the mutant is only ~1.3 kcal mol^{-1} M^{-1} (see the legend of Figure 9), whereas the *m* value for the $U \rightleftarrows N$ process for the wild-type protein is ~3.0 kcal mol^{-1} M^{-1} (Pace et al., 1990). If the U′ state of our model were indeed the completely unfolded state, i.e. U, this would imply that I_N has only about 40% of the buried surface area of the native protein. This seems unlikely, given that it has inhibitor binding properties similar to those of the native species and that, in the wild-type protein, I_N is indistinguishable from N by absorbance measurements. It is also unlikely that this difference is due to the Trp mutation; the dependence of unfolding by GdnHCl is almost identical for the wild-type and mutant proteins as shown by the overlapping GdnHCl dependence curves (Figure 3). If the introduction of the Trp residue significantly altered the exposed surface area of the folded or unfolded state, the GdnHCl transition would presumably be very different from that of the wild-type protein. One contributing factor is the contribution that U_s^I makes to the equilibrium *m* value for the $U' \rightleftarrows I_N$ process (U′ is a sum of all unfolded states). However, given the relatively small population of U_s^I (17%), it is unlikely that this can completely account for this discrepancy.

A second possible explanation for the small *m* value of the $U' \rightleftarrows I_N$ process is that the structure formed in the burst phase (U′) has significant buried surface area. Such an explanation would also serve to resolve a similar discrepancy in the refolding of U_{vf} in which Houry et al. (1995) observed that there was a substantial difference (~40%) in the amount of buried surface area in the folding and unfolding transition states. This explanation, however, requires that the intermediate formed in the burst phase (U′) contain a substantial amount of buried surface area. Its insensitivity to GdnHCl concentrations up to 2.6 M would, therefore, indicate substantial stability. Further investigation is clearly warranted to resolve this point.

Isomerization Rates. In the kinetic model, k_3 corresponds to the rate constant for isomerization of the Trp92−Pro93 peptide bond in I_N. Given that the rate of cis/trans proline isomerization in the unfolded state is generally considered to be insensitive to denaturant concentration (Nall, 1985), the steep dependence of k_3 on GdnHCl concentration (Figure 9C) seems surprising. However, the cis/trans isomerization process corresponding to k_3 occurs in a protein in a native-like conformation. This could lead to significant alterations in the rate of proline isomerization due to specific tertiary interactions; such effects have been observed in other proteins (Kiefhaber et al., 1992; Texter et al., 1992). Moreover, Cook et al. (1979) have measured the GdnHCl dependence of the rate of cis/trans isomerization of Pro93 in the I_N intermediate during the refolding of wild-type RNase A. These measurements were made by the use of triple-jump experiments. Their results are consistent with the GdnHCl dependence that we observe for k_3.

Double-Jump Studies. In addition to the magnitude of the burst phase which was discussed above, a comparison of the rate constants for the refolding of U_{vf} can provide important information about the folding process. The rate of refolding of the Trp mutant is significantly faster than that of wild-type RNase A (Table 3). This is particularly evident at 2.5 M GdnHCl where the refolding rate constant (τ^{-1}) of the Trp mutant is twice that of the wild-type protein. The refolding process that occurs in the double-jump experiment (Houry et al., 1995) is

$$U_{vf} \rightleftharpoons I_\Phi \rightarrow [\text{transition state}] \rightarrow N \qquad (3)$$

Therefore, it is the stability of I_Φ and N that dictate the folding rate. The fact that the Trp mutant folds significantly faster than the wild-type protein could be interpreted as a stabilization of I_Φ in the Trp mutant, thereby leading to an acceleration of the folding rate. Alternatively, some interaction, which normally must be broken during the refolding of the wild-type protein, may be disrupted in the Trp mutant. The first explanation appears more likely since the effect is greater at high GdnHCl concentration where the population of I_Φ in the refolding of *wild-type* RNase A is known to be small. This would, therefore, seem to suggest that the presence of I_Φ accelerates the folding process. This argument is strengthened further when the unfolding data are considered. The Trp mutant unfolds more slowly than the wild type, indicating that Trp92 stabilizes the native conformation. The proposal that the interactions involving Trp92 in I_Φ are native-like is also supported by the fact that there is a decrease in the fluorescence in the burst phase; quenching of fluorescence is indicative of going from a non-native to a native state.

CONCLUSIONS

The substitution of tryptophan for Tyr92 did not appear to alter the structure of RNase A substantially as shown by enzymatic activity and equilibrium denaturation. The mutation enabled us to obtain site-specific information about the folding of the protein through single- and double-jump folding studies. The hydrophobically collapsed intermediate I_Φ was observed directly, which is not possible with wild-type RNase A. These studies indicate that the region around

Trp92 is involved in the formation of I_Φ, supporting the theory that this region is part of a chain-folding initiation site. In addition, a GdnHCl-independent burst phase, which may arise from local interactions involving the Trp92 residue, was detected. Single-jump folding studies allowed direct observation of a native-like intermediate (I_N). Refolding data at different final GdnHCl concentrations were fit to a kinetic model which was simpler than the current model for the folding of wild-type RNase A but was not inconsistent with what is currently known about the folding pathway. This model supports the view that the isomerization of the Tyr92−Pro93 bond is involved in the folding pathway of the slow refolding species.

ACKNOWLEDGMENT

We thank J. H. Laity for assistance in preparation of the Trp mutant. We also thank R. W. Dodge for kindly providing and modifying his fitting programs and E. E. DiBella for providing helpful advice throughout this project.

APPENDIX

Kinetic Analysis of Folding Data

Folding Species. We model the fluorescence data with a minimal model, the simplest kinetic model consistent with experiment. The first step is to estimate the number of folding species. If the folding proceeds by unimolecular reactions, the number of folding species equals the number of exponentials in the fluorescence signal. The proof is as follows.

Consider a system of unimolecular reactions with p chemical species. The rate equations for their concentrations c_i can be written in matrix form

$$\frac{d\mathbf{c}}{dt} \equiv \frac{d}{dt}\begin{pmatrix} c_1 \\ c_2 \\ \dots \\ c_p \end{pmatrix} = -\mathbf{M}\mathbf{c} \tag{A-1}$$

The general analytic solution can be written as (Arnold, 1973)

$$\mathbf{c}(t) = \sum_{k=1}^{p} \mathbf{r}_k(\mathbf{l}_k \cdot \mathbf{c}_0)e^{-\lambda_k t} \tag{A-2}$$

where the λ_k values are the eigenvalues of the rate matrix $\mathbf{M}$, $\mathbf{r}_k$ and $\mathbf{1}_k$ are its right and left eigenvectors, respectively, and $\mathbf{c}_0$ is the vector of initial concentrations. Barring accidental degeneracies, a $p \times p$ transition rate matrix has p eigenvalues, one of which must be 0 by conservation of mass. Hence, the concentrations of a p species model equal a constant plus $p - 1$ exponentials.

The fitting methods described below indicate that two exponentials and a constant suffice to model the fluorescence data, except at the highest GdnHCl concentration (2.6 M), where one exponential and a constant suffice. The χ^2 values are typically well within the assigned tolerance, and the residuals show no long-time correlations. Hence, we adopt the working hypothesis that the fluorescence data are modeled adequately by two exponentials plus a constant.

It follows that the minimal kinetic model has three folding species. Of these, one must be the native species, labeled N. The initial species is labelled U′, as described in the Discussion. The intermediate species is labeled I_N, in accord with the inhibitor binding experiments.

Minimal Model. The most general model involving U′, I_N, and N is depicted in Figure 8; the unfolded species U′ decays directly to the native species N, through an intermediate I_N. It should be noted that the reactions to the native species have been treated as irreversible since all of the measurements were made under baseline folding conditions (see Figure 3).

The rate equation for this kinetic model can be solved analytically. The fluorescence intensity $F(t)$ equals a constant plus two decaying exponentials

$$F(t) = F_\infty + A_1 e^{-\lambda_1 t} + A_2 e^{-\lambda_2 t} \tag{A-3}$$

where A_1 and A_2 are the fast and slow amplitudes, respectively, λ_1 and λ_2 are the fast and slow decay rate constants. These (observed) amplitudes and decay rate constants are related to the quantum yields and reaction rate constants of the model by five simple equations

$$F_\infty = Q_N \tag{A-4}$$

$$A_1 + A_2 = Q_U - Q_N \tag{A-5}$$

$$\lambda_1 + \lambda_2 = k_1 + k_2 + k_3 + k_4 \tag{A-6}$$

$$\lambda_1\lambda_2 = k_1k_3 + k_4(k_2 + k_3) \tag{A-7}$$

$$\lambda_1A_1 + \lambda_2A_2 = k_1(Q_U - Q_{I_N}) + k_4(Q_U - Q_N) \tag{A-8}$$

These equations are derived below, after their application is discussed.

By fitting an observation run to a sum of exponentials, we can obtain the amplitudes and decay rate constants. These quantities determine the left-hand sides of equations A-4−A-8, giving five simple equations for the quantum yields and reaction rate constants of the model. However, since the model has seven unknowns, the model cannot be solved completely without additional information, e.g. parameter values derived from other experiments or from *a priori* constraints.

Such constraints on the reaction rate constants can be provided by the physical mechanism of the reaction. For example, one rate constant may be known to be negligibly small under given experimental conditions and can be set to 0. Alternatively, the model can be parametrized from data taken under different conditions, by assuming a functional form for certain rate constants. The latter procedure was adopted here, by requiring that the rate constants k_1 and k_2 vary exponentially with GdnHCl concentration, as explained in the Discussion.

Solving the Minimal Model Analytically. The rate equation of the minimal model can be written

$$\frac{d\mathbf{c}}{dt} \equiv \frac{d}{dt}\begin{pmatrix} U' \\ I \\ N \end{pmatrix} = \begin{bmatrix} -k_1-k_4 & k_2 & 0 \\ k_1 & -k_2-k_3 & 0 \\ k_4 & k_3 & 0 \end{bmatrix}\begin{pmatrix} U' \\ I \\ N \end{pmatrix} = -\mathbf{M}\mathbf{c} \tag{A-9}$$

Solving the secular equation gives the eigenvalues of the rate matrix $\mathbf{M}$

$$\lambda_0 = 0 \tag{A-10}$$

$$\lambda_1 = {}^1/_2(\sigma + \sqrt{\sigma^2 - 4\rho}) \tag{A-11}$$

$$\lambda_2 = {}^1/_2(\sigma - \sqrt{\sigma^2 - 4\rho}) \tag{A-12}$$

where $\sigma \equiv k_1 + k_2 + k_3 + k_4$ and $\rho \equiv k_1k_3 + k_4(k_2 + k_3)$. It should be noted that λ_1 corresponds to the faster decay and λ_2 to the slower. These solutions yield eqs A-6 and A-7 above.

The corresponding right eigenvectors of **M** can be written

$$\mathbf{r_0} = [0,0,1] \tag{A-13}$$

$$\mathbf{r_1} = [\eta_1,k_1,-k_1 - \eta_1] \tag{A-14}$$

$$\mathbf{r_2} = [\eta_2,k_1,-k_1 - \eta_2] \tag{A-15}$$

where $\eta_{1,2} \equiv k_2 + k_3 - \lambda_{1,2}$. The left and right eigenvectors are required to obey the normalization condition

$$\mathbf{r_m}\cdot\mathbf{1_n} = \begin{cases} 0 & \text{if } m \neq n \\ 1 & \text{if } m = n \end{cases} \tag{A-16}$$

which uniquely determines the left eigenvectors

$$\mathbf{1_0} = [1, 1, 1] \tag{A-17}$$

$$\mathbf{1_1} = [-k_1,\eta_2,0]H \tag{A-18}$$

$$\mathbf{1_2} = [k_1,-\eta_1,0]H \tag{A-19}$$

where $H \equiv 1/k_1(\lambda_1 - \lambda_2)$.

Since the concentrations have been normalized to unity, and since the protein exists initially only as the species U' (by assumption), the initial concentration vector is

$$\mathbf{c_0} \equiv \begin{pmatrix} U' \\ I \\ N \end{pmatrix}_{t=0} = \begin{pmatrix} 1 \\ 0 \\ 0 \end{pmatrix} \tag{A-20}$$

Given the eigenvalues, the right and left eigenvectors, and the initial concentration vector, the concentrations can be computed for any time, using the solution

$$\mathbf{c}(t) = \sum_{k=0}^{2} \mathbf{r_k}(\mathbf{1_k}\cdot\mathbf{c_0})e^{-\lambda_k t} \tag{A-21}$$

Hence, the concentrations can be expressed as analytic functions of the four rate constants and the initial concentrations of the model.

The solution for the fluorescence intensity $F(t)$ can be obtained similarly. Denoting the quantum yields as $\{Q_{U'}, Q_{I_N}, Q_N\}$, we can express the fluorescence intensity as

$$F(t) = Q_{U'}U'(t) + Q_{I_N}I_N(t) + Q_N N(t) \equiv \mathbf{Q}\cdot\mathbf{c}(t) \tag{A-22}$$

Substituting the solution (A-21) for $\mathbf{c}(t)$ yields

$$F(t) = \sum_{k=0}^{2} (\mathbf{Q}\cdot\mathbf{r}_k)(\mathbf{1_k}\cdot\mathbf{c_0})e^{-\lambda_k t} \equiv \sum_{k=0}^{2} A_k e^{-\lambda_k t} \tag{A-23}$$

where $A_k \equiv (\mathbf{Q}\cdot\mathbf{r_k})(\mathbf{1_k}\cdot\mathbf{c_0})$. As shown above, one eigenvalue is always 0, corresponding to the conservation of mass. Hence, the fluorescence intensity is the sum of a constant plus two exponentials (eq A-3) where

$$F\infty = (\mathbf{Q}\cdot\mathbf{r_0})(\mathbf{1_0}\cdot\mathbf{c_0}) \tag{A-24}$$

$$A_1 = (\mathbf{Q}\cdot\mathbf{r_1})(\mathbf{1_1}\cdot\mathbf{c_0}) \tag{A-25}$$

$$A_2 = (\mathbf{Q}\cdot\mathbf{r_2})(\mathbf{1_2}\cdot\mathbf{c_0}) \tag{A-26}$$

Given the initial concentrations, and the right and left eigenvectors, these equations may be written out explicitly as

$$F_\infty = Q_N \tag{A-27}$$

$$A_1 = -k_1\eta_1 H(Q_{U'} - Q_N) - {k_1}^2 H(Q_{I_N} - Q_N) \tag{A28}$$

$$A_2 = +k_1\eta_2 H(Q_{U'} - Q_N) + {k_1}^2 H(Q_{I_N} - Q_N) \tag{A-29}$$

Combination of these solutions with those for the rate constants yields the five equations (A-4−A-8). Analogous equations can be derived for four-species models.

Numerical Fits to the Minimal Model. The numerical fits to the minimal model minimized the χ^2 statistic by simulated annealing, in concert with the Nelder−Mead simplex method (Press et al., 1992) and a novel Monte Carlo method (W. J. Wedemeyer and H. A. Scheraga, in preparation).

Uncertainties in the fluorescence intensity were estimated by evaluating the difference between the fluorescence intensities of runs taken under identical experimental conditions:

$$\sigma^2_{\text{model}}(t) \equiv \frac{1}{R-1}\sum_{s=1}^{R}[F_s(t) - F_{\text{avg}}(t)]^2 \tag{A-30}$$

where the sum is taken over R observation runs. In equation A-30, $F_s(t)$ denotes the fluorescence intensity observed in run s at time t, whereas $F_{\text{avg}}(t)$ represents the average of all the fluorescence intensities observed at time t.

$$F_{\text{avg}}(t) = \frac{1}{R}\sum_{s=1}^{R} F_s(t) \tag{A-31}$$

This method of estimating uncertainties allows time-varying errors, e.g. mixing artifacts, to be modeled statistically. The χ^2 statistic was computed normally

$$\chi^2 \equiv \sum_{\text{all data}}\left[\frac{F(t) - F_{\text{pred}}(t)}{\sigma_{\text{model}}(t)}\right]^2 \tag{A-32}$$

where $F_{\text{pred}}(t)$ is the fluorescence intensity predicted by the model under the given experimental conditions.

Twenty-one parameters were varied to minimize χ^2. Specifically, the rate constants k_1 and k_2 were required to vary exponentially with the GdnHCl concentration

$$k_1 = {k_1}^0 \exp\left(-\frac{m_1[\text{GdnHCl}]}{RT}\right) \tag{A-33}$$

$$k_2 = {k_2}^0 \exp\left(-\frac{m_2[\text{GdnHCl}]}{RT}\right) \tag{A-34}$$

yielding four parameters: ${k_1}^0$, ${k_2}^0$, m_1, and m_2. The quantum

yield differences were assumed to be independent of GdnHCl concentration, giving two more parameters

$$\Delta Q_1 \equiv Q_N - Q_{U'} \quad \text{(A-35)}$$

$$\Delta Q_2 \equiv Q_{U'} - Q_I \quad \text{(A-36)}$$

The remaining 15 parameters resulted by allowing three parameters (k_3, k_4, and Q_N) to vary independently for each of the five guanidine concentrations. The parameter Q_N was allowed to vary with GdnHCl concentration to allow for scattering by the GdnHCl itself; only small differences in Q_N were observed.

The model was fit simultaneously to all the observation runs. The final reduced χ^2 for the fitting was 0.991, well within 2.5 standard deviations. Hence, the proposed minimal model fits the fluorescence data excellently.

We also attempted to fit models with only three reactions, but their final χ^2 could not be minimized to within 2.5 standard deviations. Therefore, the four-reaction model described above is indeed the "minimal model" fitting the experimental data.

The errors in the fitted parameters were obtained as follows. Each of the 21 parameters in turn was set to values departing from its best-fit value. The other 20 parameters were then varied, holding this parameter fixed, to reminimize χ^2. The values of the limits were adjusted to bring the reminimized χ^2 to a 95% confidence level.

It should be noted that no upper bound could be placed on the rate constant k_3 at the highest GdnHCl concentration. Even with an unphysically large k_3 (e.g. 2×10^4 s^{-1}) the reduced χ^2 could be minimized below 1.0 by adjusting the other parameters. In other words, the fluorescence data at 2.6 M GdnHCl do not limit this k_3 to a closed interval, but merely set a lower bound. This reflects the physical fact that, at 2.6 M GdnHCl, the direct folding reaction $U' \rightarrow N$ dominates over the indirect folding pathway $U' \rightleftarrows I_N \rightarrow N$. It is also for this reason that only one exponential, corresponding to k_4, is discernible at 2.6M GdnHCl.

Fitting to Exponentials. Our analysis depended critically on estimating the number of folding species by computing the minimal number of exponentials observable in the fluorescence data. The conclusion of two independent analyses was that only two decaying exponentials are discernible in the fluorescence data, except at the highest GdnHCl concentration, where only one decaying exponential is discernible.

The first analysis was a simple χ^2 fitting to exponentials. The fluorescence data were successively fit to ever larger numbers of exponentials until the minimized χ^2 fell within 2.5 standard deviations of its expected mean. As above, the χ^2 function was minimized with simulated annealing, combined with the Nelder-Mead simplex method (Press et al., 1992) and a novel Monte Carlo method (W. J. Wedemeyer and H. A. Scheraga, in preparation). This method indicated that only two decaying exponentials are discernible within the data, except at the highest GdnHCl concentration, where only one exponential is discernible.

The uncertainty in an observation run was estimated as follows. A quantity (L_i) was computed from three successive fluorescence intensities

$$L_i \equiv 2F_i - F_{i-1} - F_{i+1} \quad \text{(A-37)}$$

corresponding to the local second derivative. Assuming that the noise in the data is uncorrelated and drawn from the same distribution at every point, the rms uncertainty is given by

$$\sigma^2_{exp} = {}^1/_6(\langle L^2 \rangle - \langle L \rangle^2) \quad \text{(A-38)}$$

where broken brackets represent averaging over all data within a run. The χ^2 statistic for fitting exponentials to a single observation run is therefore

$$\chi^2 = \sum_{\text{all data}} \left[\frac{F(t) - F_{pred}(t)}{\sigma_{exp}} \right]^2 \quad \text{(A-39)}$$

where $F_{pred}(t)$ is the fluorescence intensity predicted by a given set of exponential amplitudes and decay rate constants.

The second analysis employed de Prony's method (Magar, 1972), as modified in our laboratory to reduce its sensitivity to noise. The de Prony method can be considered as a generalization of the well-known log-linear plot used for fitting a single exponential. The de Prony method allows data to be fit deterministically to an arbitrary number M of exponentials. The drawback, however, is that the extracted exponentials may be oscillatory (sine and cosine functions) or even exponentially growing. These other exponentials serve to mimic the noise in the data.

For this study, M was set successively from 1 to 50 for each observation run. Only the decaying exponentials were retained; exponentially growing and oscillatory exponentials were rejected. For all values of M, the number of decaying exponentials never exceeded two. Hence, the de Prony method also finds that only two decaying exponentials are discernible in the data.

Both analysis methods agree that the fluorescence data exhibit at most two decaying exponentials. All other signals are statistically equivalent to noise. Hence, the minimal model possesses only three distinct species.

REFERENCES

Alonso, D. O. V., & Dill, K. A. (1991) *Biochemistry 30*, 5974−5985.

Arnold, V. I., (1973) *Ordinary Differential Equations*(Silverman, R. A., Ed.) MIT Press, pp 115−118, Cambridge, MA.

Bottomley, S. P., Popplewell, A. G., Scawen, M., Wan, T., Sutton, B. J., & Gore, M. G.(1994) *Protein Eng. 7*, 1463−1470.

Burstein, E. A., Vedenkina, N. S., & Ivkova, M. N. (1973) *Photochem. Photobiol. 18*, 263−279.

Choi, S.-G., O'Donnell, S. E., Sarken, K. D., & Hardman, J. K. (1995) *J. Biol. Chem. 270*, 17712−17715.

Cook, K. H., Schmid, F. X., & Baldwin, R. L. (1979) *Proc. Natl. Acad. Sci. U.S.A. 76*, 6157−6161.

Crook, E. M., Mathias, A. P., & Rabin, B. R. (1960) *Biochem. J. 74*, 234−238.

Denton, J. B., Konishi, Y., & Scheraga, H. A. (1982) *Biochemistry 21*, 5155−5163.

Dodge, R. W., & Scheraga, H. A. (1996) *Biochemistry 35*, 1548−1559.

Dodge, R. W., Laity, J. H., Rothwarf, D. M., Shimotakahara, S., & Scheraga, H. A. (1994) *J. Protein Chem. 13*, 409−421.

Edelhoch, H., & Lippoldt, R. E. (1969) *J. Biol. Chem. 244*, 3876−3883.

Eftink, M. R (1991) *Methods Biochem. Anal. 35*, 127−205.

Garcia, P., Desmadril, M., Minard, P., & Yon, J. M. (1995) *Biochemistry 34*, 397−404.

Garel, J.-R., & Baldwin, R. L. (1973) *Proc. Natl. Acad. Sci. U.S.A. 70*, 3347−3351.

Garel, J.-R., Nall, B. T., & Baldwin, R. L. (1976) *Proc. Natl. Acad. Sci. U.S.A. 73*, 1853−1857.

Houry, W. A., & Scheraga, H. A. (1996) *Biochemistry 35*, 11719−11733.
Houry, W. A., Rothwarf, D. M., & Scheraga, H. A. (1994) *Biochemistry 33*, 2516−2530.
Houry, W. A., Rothwarf, D. M., & Scheraga, H. A. (1995) *Nat. Struct. Biol. 2*, 495−503.
Houry, W. A., Rothwarf, D. M., & Scheraga, H. A. (1996) *Biochemistry 35*, 10125−10133.
Kaiser, H. (1970) *Anal. Chem. 42*, 24A.
Kemmink, J., & Creighton, T. E. (1995) *J. Mol. Biol. 245*, 251−260.
Kiefhaber, T., Grunert, H.-P., Hahn, U., & Schmid, F. X. (1992) *Proteins: Struct., Funct., Genet. 12*, 171−179.
Konishi, Y., & Scheraga, H. A. (1980) *Biochemistry 19*, 1308−1316.
Kronman, M. J., & Holmes, L. G. (1971) *Photochem. Photobiol. 14*, 113−134.
Laity, J. H., Shimotakahara, S., & Scheraga, H. A. (1993) *Proc. Natl. Acad. Sci. U.S.A. 90*, 615−619.
Leach, S. J., & Scheraga, H. A. (1960) *J. Biol. Chem. 235*, 2827−2829.
Lin, L.-N., & Brandts, J. F. (1983) *Biochemistry 22*, 559−563.
Magar, M. E. (1972) *Data Analysis in Biochemistry and Biophysics*, pp 161−162, Academic Press, New York.
Matheson, R. R., Jr., & Scheraga, H. A. (1978) *Macromolecules 11*, 819−829.
Montelione, G. T., & Scheraga, H. A. (1989) *Acc. Chem. Res. 22*, 70−76.
Nall, B. T. (1985) *Comments Mol. Cell. Biophys. 3*, 123−143.
Nozaki, Y. (1972) *Methods Enzymol. 26*, 43−50.
Pace, C. N. (1986) *Methods Enzymol. 131*, 266−280.
Pace, C. N., Shirley, B. A., & Thomson, J. A. (1989) in *Protein Structure* (Creighton, T. E., Ed.) pp 311−330, IRL Press, Oxford.
Pace, C. N., Laurents, D. V., & Thomson, J. A. (1990) *Biochemistry 29*, 2564−2572.
Press, W. H., Teukolsky, S. A., Vetterling, W. T., & Flannery, B. P. (1992) *Numerical Recipes in C*, 2nd ed., pp 451−455, Cambridge University Press, Cambridge.
Rehage, A., & Schmid, F. X. (1982) *Biochemistry 21*, 1499−1505.
Roper, D. I., Moreton, K. M., Wigley, D. B., & Holbrook, J. J. (1992) *Protein Eng. 5*, 611−615.
Rothwarf, D. M., & Scheraga, H. A. (1993) *Biochemistry 32*, 2671−2679.
Schellman, J. A. (1987) *Annu. Rev. Biophys. Biophys. Chem. 16*, 115−137.
Scheraga, H. A. (1967) *Fed. Proc. 26*, 1380−1387.
Schmid, F. X. (1981) *Eur. J. Biochem. 114*, 105−109.
Schmid, F. X. (1983) *Biochemistry 22*, 4690−4696.
Schmid, F. X. (1986) *Methods Enzymol. 131*, 70−82.
Schmid, F. X., & Baldwin, R. L. (1979) *J. Mol. Biol. 133*, 285−287.
Schmid, F. X., & Blaschek, H. (1981) *Eur. J. Biochem. 114*, 111−117.
Schultz, D. A., Schmid, F. X., & Baldwin, R. L. (1992) *Protein Sci. 1*, 917−924.
Sela, M., & Anfinsen, C. B. (1957) *Biochim. Biophys. Acta. 24*, 229−235.
Smith, C. J., Clarke, A. R., Chia, W. N., Irons, L. I., Atkinson, T., & Holbrook, J. J. (1991) *Biochemistry 30*, 1028−1036.
Steer, B. A., & Merrill, A. R. (1995) *Biochemistry 34*, 7225−7233.
Texter, F. L., Spencer, D. B., Rosenstein, R., & Matthews, C. R. (1992) *Biochemistry 31*, 5687−5691.
Thannhauser, T. W., Konishi, Y., & Scheraga, H. A. (1987) *Methods Enzymol. 143*, 115−119.
Tsong, T. Y., Baldwin, R. L., & Elson, E. L. (1972) *Proc. Natl. Acad. Sci. U.S.A. 69*, 1809−1812.
Wlodawer, A., Bott, R., & Sjölin, L. (1982) *J. Biol. Chem. 257*, 1325−1332.
Wlodawer, A., Svensson, L. A., Sjölin, L., & Gilliland, G. L. (1988) *Biochemistry 27*, 2705−2717.

BI961280R